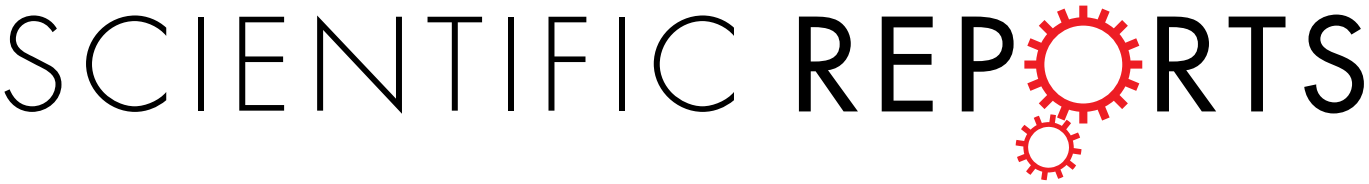

OPEN

Deformation mechanism of innovative 3D chiral metamaterials

Wenwang Wu[1,2], Dexing Qi[1,2], Haitao Liao[1,2], Guian Qian[3], Luchao Geng[4], Yinghao Niu[1,2] & Jun Liang[1,2]

Received: 25 January 2018
Accepted: 31 July 2018
Published online: 22 August 2018

Rational design of artificial microstructured metamaterials with advanced mechanical and physical properties that are not accessible in nature materials is very important. Making use of node rotation and ligament bending deformation features of chiral materials, two types of innovative 3D chiral metamaterials are proposed, namely chiral- chiral- antichiral and chiral- antichiral- antichiral metamaterials. *In-situ* compression and uniaxial tensile tests are performed for studying the mechanical properties and deformation mechanisms of these two types of 3D chiral metamaterials. Novel deformation mechanisms along different directions are explored and analyzed, such as: uniform spatial rotation deformation, tensile-shearing directed (compression-shearing directed), tensile-expansion directed (compression-shrinkage directed) deformation mechanisms of 3D chiral metamaterials, and competitions between different types of deformation mechanisms are discussed. The proposed 3D chiral metamaterials represents a series of metamaterials with robust microstructures design feasibilities.

Rational design of artificial micro architected metamaterials with advanced mechanical and physical properties that are not accessible in nature materials is challenging and important. Artificially designed metamaterials are usually arranged in repeating patterns, at scales that are smaller than the wavelengths of the phenomena they influence. The smart properties of metamaterials origin from artificially designed structures at sub-wavelength scales, and can be tailored and tuned precisely with their architected shape, geometry, size, orientation and arrangements. The interactions between architected microstructures of metamaterials and electromagnetic, sound and optical waves will result in blocking, absorbing, enhancing, or bending of waves. It has been demonstrated that rationally designed metamaterials have promising multifunctional applications, such as ultralow mass densities and ultrastrong metamaterials[1–5], sound and vibration attenuation metamaterials[6,7], electromagnetic cloaking metamaterials[8,9], negative thermal expansion metamaterials[10,11], subwave length optical metamaterials[12–15], etc.

As a special type of mechanical metamaterials, auxetic metamaterials with negative Poisson ratio can expand its volume when stretched, and the concept of auxetic materials with negative Poisson ratio was firstly described by Love in 1944 for the first time[16]. Auxetic metamaterials exhibit enhanced mechanical properties over conventional materials, such as higher shearing modulus, increased indentation resistance, good absorption properties and higher fracture toughness. Auxetic materials can be applied for designing innovative multifunctional structures, such as: body armor, packing material, knee and elbow pads, robust shock absorbing material and sponge mops. According to the geometrical relations of auxetic unit cell, there are mainly three types of auxetic materials: reentrant materials, rigid square rotation materials and chiral structures[17]. Chiral structures stands for a series of structures which cannot be mapped onto its mirror image by rotations and translations alone[18], and various types of chiral structures exist commonly in nature, such as: DNA, RNA, chiral carbon nanotube, twisting flower petals and stems, plant climbing tendrils and twisted leaves, chiral cellulose[19–21]. Besides these chiral materials in nature, various types of multifunctional artificial chiral metamaterials are designed and fabricated as well. Because of their lack of mirror symmetry, chiral metamaterials[22,23] have recently enabled several remarkable phenomena, such as negative refractive index[24], superchiral light[25], and use as broadband circular polarizers[26,27] or detectors[28].

[1]Institute of Advanced Structure Technology, Beijing Institute of Technology, Beijing, 100081, China. [2]Beijing Key Laboratory of Lightweight Multi-functional Composite Materials and Structures, Beijing, 100081, China. [3]Laboratory for Nuclear Materials, Paul Scherrer Institute, Villigen PSI, 5232, Switzerland. [4]State Key Laboratory for Turbulence and Complex Systems, College of Engineering, Peking University, Beijing, 100871, China. Correspondence and requests for materials should be addressed to W.W. (email: wuwenwang2014@163.com) or H.L. (email: ht0819@163.com) or G.Q. (email: guian.qian@psi.ch)

3D chiral metamaterials No.		L(mm)	d(mm)	t(mm)	N_x	N_y	N_z
Chiral-chiral-antichiral	A	10	5	1	6	6	6
	B	10	6	1.5	5	5	5
Chiral-antichiral-antichiral	A	12	5	1	6	6	6
	B	10	6	1.5	6	6	6

Table 1. Geometrical parameters for the two types of 3D chiral metamaterials samples (ligament length L; node width d; ligament thickness t; Number of nodes along x direction N_x; Number of nodes along y direction N_y; Number of nodes along z direction N_z).

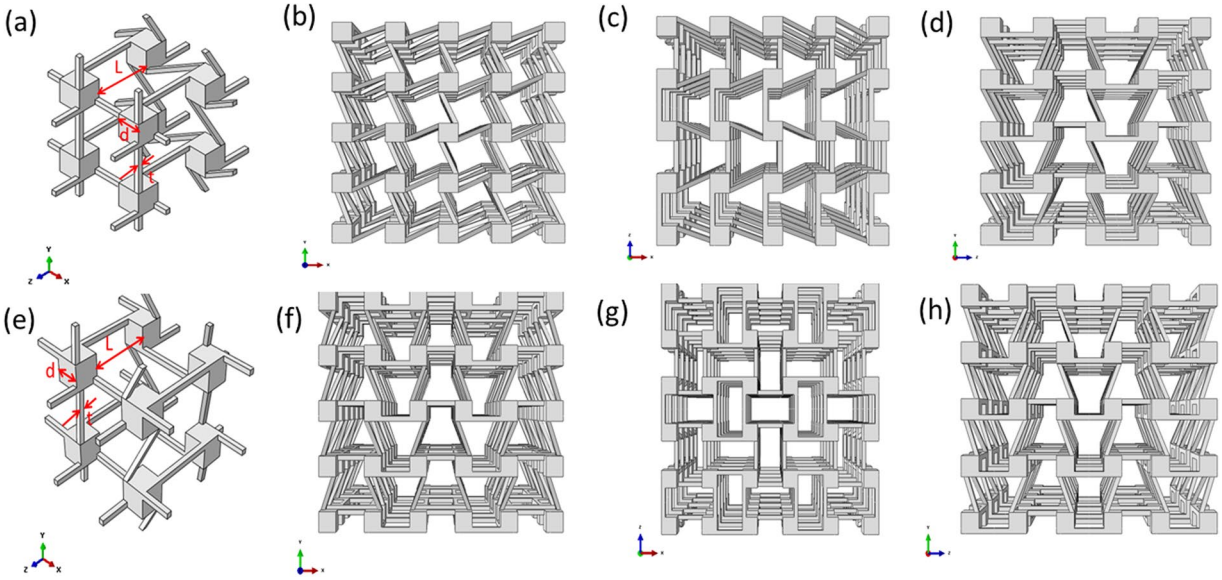

Figure 1. The x-y, y-z, z-x and stereo views of the architected 3D chiral matamaterials (**a**,**b**,**c**) and (**d**) chiral-chiral- antichiral metamaterials; (**e**,**f**,**g**) and (**h**) chiral- antichiral- antichiral metamaterials.

The mechanical properties of chiral structures can be investigated with different theoretical approaches, such as: strain energy homogenization method, internal external force equilibrium of unit cell, Cosserat (micro-polar) elasticity, etc[29–34]. In the classical theory of elasticity, the degrees of freedom are not included for describing the mechanical behaviors of microstructured solid where the microstructure characteristic length is comparable to the solid structure[35]. Due to the additional degrees of freedom allowed by internal microstructures, chiral Cosserat solids have different mechanical behaviors from solids with a center of symmetry[35–37], The Cosserat (also called micropolar) elasticity theory of Eringen[37] demonstrated robust efficiency and reliability in the modeling of materials with microstructures, such as: granular or fibrous materials, bone microstructure, or 3D lattice structures, etc. For example, based on the micropolar theory and tensor analysis, Liu *et al.*[38] developed a continuum theory for describing the dilatation–rotation coupling and shear–rotation coupling deformation mechanism of 2D chiral lattice structures. Chen *et al.*[39] proposed a micropolar continuum model for describing the constitutive relation for tetrachiral lattice structure, where 13 independent material constants are employed. Spadoni *et al.*[40] proposed a micropolar continuum model for analyzing the in-plane properties of hexachiral structures, where deformable-ring node model are employed.

Recently, Kang *et al.*[41] exploited the buckling introduced mechanical instabilities in surface-attached cellular structure, and effects of cellular unit cell geometrical parameters on the formed chiral pattern during the swelling and shrinkage cycle are studied systematically. Shan *et al.*[42] proposed an elastomeric porous metamaterials, where multiple pattern transformations can be induced by buckling. The proposed periodic porous elastic structures can generate mechanical instabilities, and can be used to tune the propagation of elastic waves in phononic crystals, enhancing the tunability of the dynamic response of the system. Ha *et al.*[43,44] proposed an innovative isotropic 3D tetrachiral metastructure, and studied its mechanical properties via finite element analysis. Fu *et al.*[45] developed the equivalent modulus and Poisson ratio of a novel 3D chiral structures made up of orthogonal assembled 2D chiral honeycomb with four ligaments. Based on the pioneering work on "missing rib" type of chiral structures designed by Smith *et al.*[46], new chiral cellular solids with center cores and softer hinges are designed and fabricated via multi-material 3D printing techniques, and amplified chirality-induced auxetic effect via elevating internal rotation efficiency can be realized[47]. Making use of the chiral rotation induced unique sequential cell-opening mechanisms, hybrid auxetic chiral mechanical metamaterial are designed, which can be employed for developing new multi-functional smart composites, sensors and/or actuators[48]. In order to overcome the twist deformation limits of linearly elastic bar, Frenzel *et al.*[49] proposed a microstructured 3D elastic chiral mechanical metamaterials

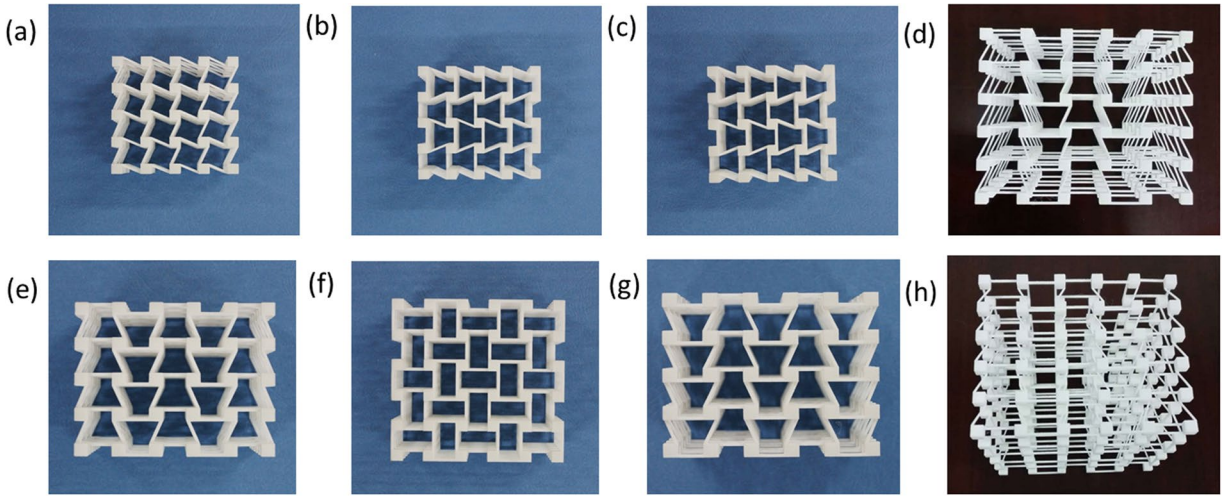

Figure 2. (**a**–**d**) x-y, y-z, z-x and stereo views of as-fabricated chiral- chiral- antichiral metamaterials; (**e**–**h**) x-y, y-z, z-x and perspective view of as-fabricated chiral- antichiral- antichiral metamaterials.

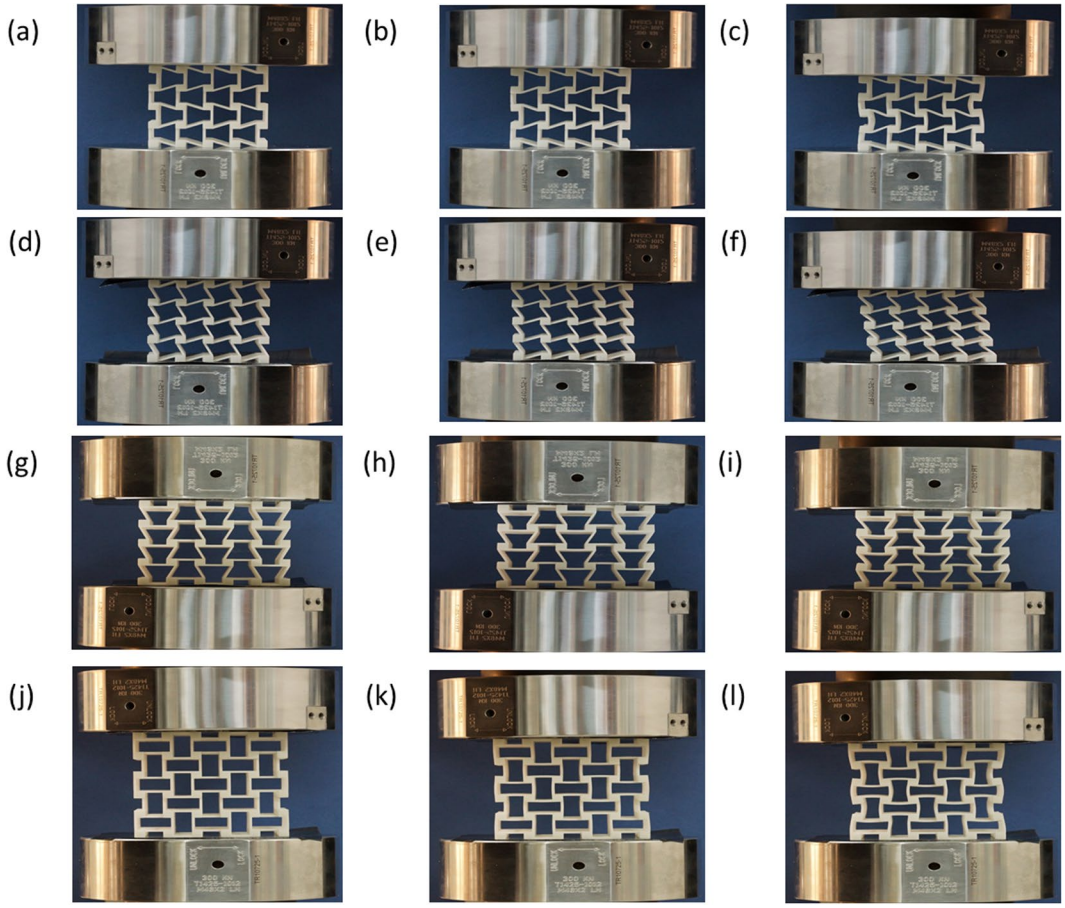

Figure 3. Deformation of 3D chiral- chiral- antichiral metamaterials under uniaxial compression test condition at different compression strain level along z antichiral direction (**a**) $\varepsilon_z = 2\%$, (b) $\varepsilon_z = 5\%$, (**c**) $\varepsilon_z = 10\%$; Deformation of 3D chiral- chiral- antichiral metamaterials under uniaxial compression test condition at different compression strain level along y chiral direction (**d**) $\varepsilon_y = 2\%$, (**e**) $\varepsilon_y = 5\%$, (f) $\varepsilon_y = 10\%$; Deformation of 3D chiral- antichiral- antichiral metamaterials under uniaxial compression test condition at different compression strain level along z chiral direction (**g**) $\varepsilon_z = 2\%$, (**h**) $\varepsilon_z = 5\%$, (**i**) $\varepsilon_z = 10\%$; Deformation of 3D chiral- antichiral- antichiral metamaterials under uniaxial compression test condition at different compression strain level along y antichiral direction (**j**) $\varepsilon_y = 2\%$, (**k**) $\varepsilon_y = 5\%$, (**l**) $\varepsilon_y = 10\%$.

Matematerials type		Chiral-chiral-antichiral		Chiral-antichiral-antichiral	
Loading axis		chiral	antichiral	chiral	antichiral
Type A	Exp	0.105	0.274	0.108	0.196
	FEA	0.139	0.384	0.155	0.240
Type B	Exp	0.559	1.526	0.823	0.981
	FEA	0.574	1.679	0.708	0.977

Table 2. Comparison between experimental and FEA simulated modulus (Unit: MPa).

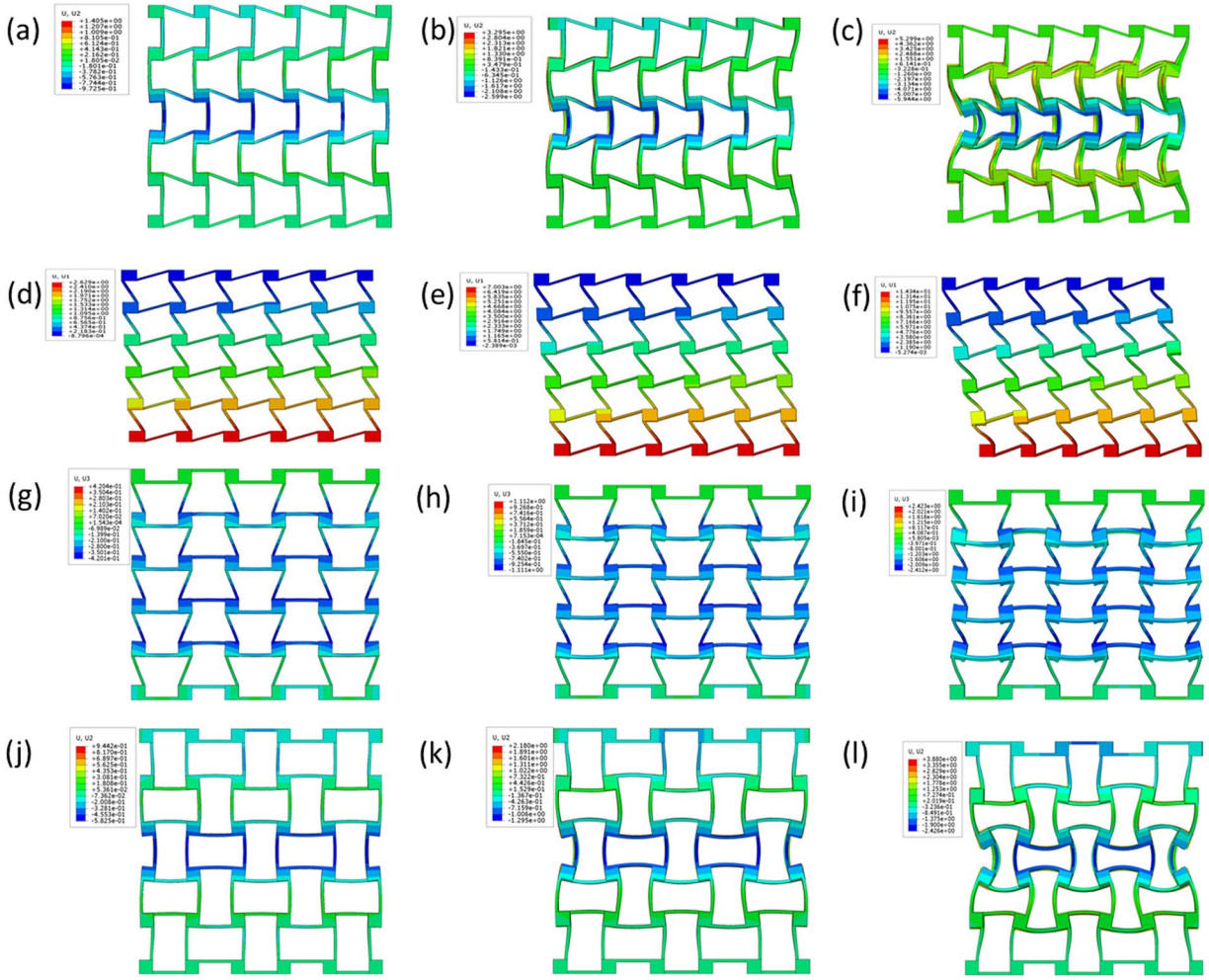

Figure 4. FEA simulated deformation of 3D chiral- chiral- antichiral metamaterials under uniaxial compression test condition at different compression strain level along z antichiral direction (**a**) $\varepsilon_z = 2\%$, (**b**) $\varepsilon_z = 5\%$, (**c**) $\varepsilon_z = 10\%$; FEA simulated deformation of 3D chiral- chiral- antichiral metamaterials under uniaxial compression test condition at different compression strain level along y chiral direction (**d**) $\varepsilon_y = 2\%$, (e) $\varepsilon_y = 5\%$, (**f**) $\varepsilon_y = 10\%$; FEA simulated deformation of 3D chiral- antichiral- antichiral metamaterials under uniaxial compression test condition at different compression strain level along z chiral direction (**g**) $\varepsilon_z = 2\%$, (**h**) $\varepsilon_z = 5\%$, (**i**) $\varepsilon_z = 10\%$; FEA simulated deformation of 3D chiral- antichiral- antichiral metamaterials under uniaxial compression test condition at different compression strain level along y antichiral direction (**j**) $\varepsilon_y = 2\%$, (**k**) $\varepsilon_y = 5\%$, (**l**) $\varepsilon_y = 10\%$.

which can realize twist deformation upon compression, the proposed tension/compression induced twist deformation has potential applications in chiral optical metamaterials, such as: optical dynamic cloaking structures. Sha *et al.*[50] proposed the design of large-scale chiral metallic glasses with extensive hardening and large ductility properties, the mechanical behaviors of the metallic glass chiral nanolattice (MGCN) can be significantly altered through changing the thickness and length of the ligaments in the nanolattices.

In this paper, depending on the geometrical relations between nodes and ligaments, two types of innovative 3D chiral metamaterials are proposed, namely chiral- chiral- antichiral, and chiral- antichiral- antichiral

3D chiral metamaterials No.	L(mm)	d(mm)	t(mm)	N_x	N_y	N_z
Chiral-chiral-antichiral	2	8	2	6	6	6
Chiral-antichiral-antichiral	2	8	2	6	6	6

Table 3. Geometrical parameters for the two types of 3D chiral metamaterials samples (ligament length L; node width d; ligament thickness t; Number of nodes along x direction N_x; Number of nodes along y direction N_y; Number of nodes along z direction N_z).

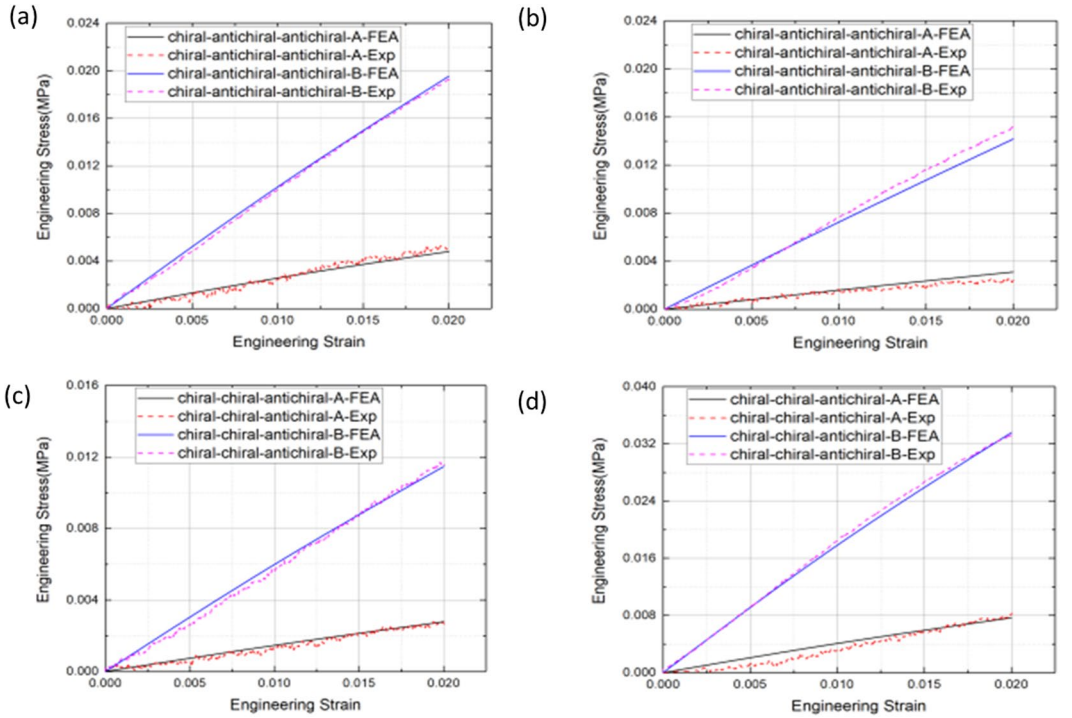

Figure 5. Experimental and FEA simulated strain-stress curves of (**a**) FEA simulated deformation of chiral-chiral- antichiral metamaterials under uniaxial compression test condition until compression strain level $\varepsilon_z = 2\%$ along z antichiral direction; (**b**) FEA simulated deformation of chiral- chiral- antichiral metamaterials under uniaxial compression test condition until compression strain level $\varepsilon_y = 2\%$ along y chiral direction; (**c**) FEA simulated deformation of chiral- antichiral- antichiral metamaterials under uniaxial compression test condition until compression strain level $\varepsilon_z = 2\%$ along z chiral direction; (**d**) FEA simulated deformation of chiral- antichiral- antichiral metamaterials under uniaxial compression test condition until compression strain level $\varepsilon_y = 2\%$ along y antichiral direction.

metamaterials. Firstly, two series of these two types of 3D chiral metamaterials with different geometrical parameters are designed, and *in-situ* compression tests are performed for studying the mechanical properties and deformation mechanisms of these two types of 3D chiral metamaterials. Novel deformation mechanisms such as: compression-shearing, compression-shrinking auxetic deformation of chiral unit cell, antichiral unit cell and chiral-antichiral hybrid unit cell along different directions are explored and analyzed. Secondly, *in-situ* uniaxial tensile tests are carried out, and competitions between different types of deformation mechanisms are discussed. With the progress of micro- and nano- manufacturing techniques, the proposed 3D chiral metamaterials show promising performances for future industrial applications, such as: sound absorption and vibration metamaterials, morphing structures, chiral optical metamaterials, shape memory actuators and biomechanical devices.

Mechanical Properties of 3D chiral metamaterials

Topological design of innovative 3D chiral metamaterials. Chiral structures are architected with circular, polygonal, elliptical, sphere or cubic nodes and ligaments connecting neighboring nodes in 2D or 3D spaces, the deformation modes of chiral metamaterials are featured by node rotation and ligaments bending deformation under external loading conditions. Depending on the geometrical relation between ligaments and nodes of 3D chiral metastructures, there are chiral and antichiral topological configurations along x, y and z directions respectively. As shown in Fig. 1, two types of 3D chiral unit cells are proposed, namely chiral- chiral-antichiral and chiral- antichiral- antichiral architected metastructures, respectively. The x-y, y-z, z-x views and stereo views of these two types of metastructures are shown in Fig. 1(a–h), respectively. The topology layout of these two types of 3D chiral metamaterials can be realized in two steps: Firstly, constructing 3D chiral unit cell; Secondly, generating the global metamaterials through periodic distribution of 3D chiral unit cells along the x,

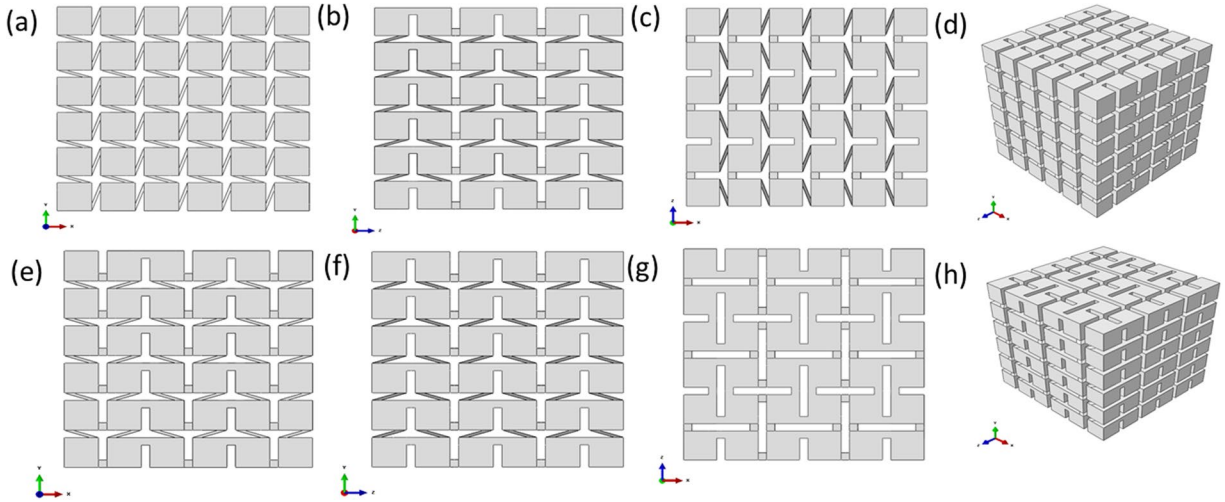

Figure 6. The x-y, y-z, z-x and stereo views of the architected 3D chiral matamaterials (**a**), (**b**), (**c**) and (**d**) chiral- chiral- antichiral metamaterials; (**e**), (**f**), (**g**) and (**h**) chiral- antichiral- antichiral metamaterials.

y, z directions. As shown in Fig. 1(a,e), the geometrical parameters for describing the 3D chiral unit cells with cubic nodes are: ligament perpendicular length L along x, y and z directions, cubic node side length d, ligaments thickness t, the numbers of unit cells along x, y and z directions are N_x, N_y and N_z respectively.

***In-situ* compression tests of 3D chiral metamaterials.** In this subsection, two series of 3D chiral metamaterials with different geometrical parameters are designed, namely Type A and Type B, respectively. The geometrical parameters of these designed two types of 3D chiral metamaterials are shown in Table 1. The two series of chiral metamaterials are fabricated with nylon powder selected laser sintering (SLS) 3D printer @ BMF Material Technology Inc. in Guang Dong Province of China, and the spatial resolution is 8 μm along x, y and z directions. Finally, Type A and Type B samples are fabricated for these two types of 3D chiral metamaterials, and the as-fabricated Type A samples are shown in Fig. 2.

Before performing compression tests of these two types of 3D chiral metamaterials, the mechanical properties of the SLS nylon material are tested. Totally, 5 uniaxial tensile samples are fabricated, and uniaxial tensile experiments are performed on an Instron®5985 machine at a displacement rate of 1 mm/min. Finally, the average elastic modulus of the 5 as-fabricated tensile samples is:$E_s = 1021.00$ MPa, where the deviation of modulus is: ±0.75 MPa, and the average ultimate strain of the material is $\varepsilon_{max} = 0.16$. After finishing the material properties tests, compression tests of two series of 3D chiral metamaterials are performed, where the loading force, displacement and deformation images during the loading process are recorded, the samples are loaded until compression strain level 10%, and deformation process of these two types of 3D chiral metastructures are shown in Fig. 3. During compression experiments, graphite sheets with quite low friction coefficients (<=0.005) are attached onto the compression contacting surfaces for minimizing the friction force. Finally, relations between axial compression strain and compression stress are generated. Meanwhile, finite element analysis (FEA) simulations of the deformation process of these two series of 3D chiral metamaterials are performed, and comparisons with experimental results are carried out for verification. In all the FEA simulation cases, uniaxial compression displacement loadings are applied on one end of the samples, while the other end of the sample is fixed, where the compression force and axial displacement during the simulation process are recorded until 10% compression strain level, the FEA simulated deformation process of these two types of chiral metamaterials are shown in Fig. 4. The experimental and FEA simulated modulus comparisons for Type A and Type B samples are calculated until 2% compression strain, and the results are shown in Table 2 and Fig. 5.

During the linearly compression process, elastic bending deformation of the ligaments and rotation of circular nodes are dominant, the chiral ligaments form full-wave deformation mode, while the antichiral ligaments form half-wave deformation mode. As shown in Figs 3(a–c) and 4(a–c), the 3D chiral- chiral- antichiral metamaterials was compressed along the antichiral direction, the chiral ligaments form full-wave deformation mode, and the anti-tetrachiral ligaments form half-wave deformation mode, demonstrating auxetic deformation behaviors. As shown in Figs 3(d–f) and 4(d–f), the 3D chiral- chiral- antichiral metamaterials was compressed along the chiral direction, the chiral ligaments form full-wave deformation mode. As shown in Figs 3 (g–i) and 4 (g–i), the 3D chiral- antichiral- antichiral metamaterials was compressed along the chiral direction, the chiral ligaments form full-wave deformation mode, and the anti-tetrachiral ligaments form half-wave deformation mode, demonstrating auxetic deformation behaviors. As shown in Figs 3 (j–l) and 4 (j–l), the 3D chiral- antichiral- antichiral metamaterials was compressed along the antichiral direction, and the anti-tetrachiral ligaments form half-wave deformation mode, demonstrating auxetic deformation behaviors. It can be seen from Figs 3 and 4 that: when these two types of chiral metamaterials are compressed along different loading directions, novel unique deformation mechanisms such as: compression-shearing deformation mechanism and auxetic deformation mechanism can be generated.

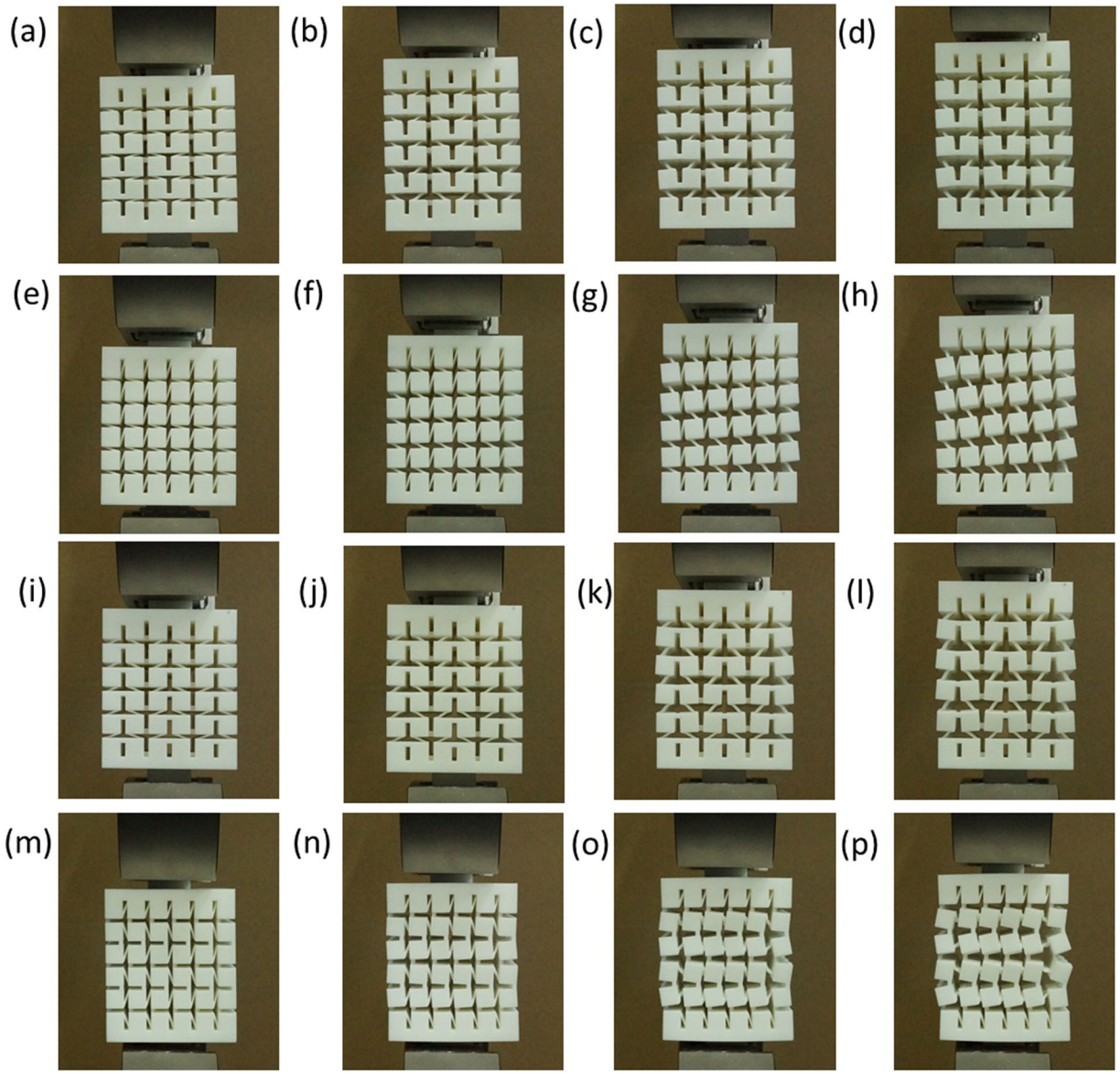

Figure 7. Deformation of chiral- chiral- antichiral metamaterials under uniaxial tensile test condition at different tensile strain level along z antichiral direction (**a**) $\varepsilon_z = 0.0\%$, (**b**) $\varepsilon_z = 10\%$, (**c**) $\varepsilon_z = 14\%$, (**d**) $\varepsilon_z = 18.9\%$; Deformation of chiral- chiral- antichiral metamaterials under uniaxial tensile test condition at different tensile strain level along y chiral direction (**e**) $\varepsilon_y = 0.0\%$, (**f**) $\varepsilon_y = 6.7\%$, (**g**) $\varepsilon_y = 14.6\%$, (**h**) $\varepsilon_y = 20.5\%$; Deformation of chiral- antichiral- antichiral metamaterials under uniaxial tensile test condition at different tensile strain level along z chiral direction (**i**) $\varepsilon_z = 4.8\%$, (**j**) $\varepsilon_z = 4.6\%$, (**k**) $\varepsilon_z = 11.5\%$, (**l**) $\varepsilon_z = 17.2\%$; Deformation of chiral- antichiral- antichiral metamaterials under uniaxial tensile test condition at different tensile strain level along y antichiral direction (**m**) $\varepsilon_y = 0.0\%$, (**n**) $\varepsilon_y = 3.3\%$, (**o**) $\varepsilon_y = 7.2\%$, (**p**) $\varepsilon_y = 9.1\%$.

Uniaxial tensile tests of 3D chiral metamaterials. In this subsection, uniaxial tensile tests are performed for exploring the deformation mechanisms of these two types of 3D chiral metamaterials. The geometrical parameters of designed two types of 3D chiral metamaterials are shown in Table 3. As shown in Fig. 6, these two types of chiral metamaterials are fabricated with nylon powder selected laser sintering (SLS) 3D printer @ BMF Material Technology Inc. in GuangDong Province of China. Afterwards, *in-situ* tensile tests of 3D chiral metamaterials are performed, where the loading force, displacement and deformation images during the loading process are recorded, and deformation process of these two types of 3D chiral metastructures are shown in Fig. 7. During the linearly straining process, elastic bending deformation of the ligaments and rotation of circular nodes are dominant, the chiral ligaments form full-wave deformation mode, while the antichiral ligaments form half-wave deformation mode. Figure 7 (a–d) show the y-z view of the 3D chiral- chiral- antichiral metamaterials strained along the chiral direction at 0.0%, 10.0%, 14.0% and 18.9% level, and Fig. 7 (e–h) show the x-z view of the 3D chiral- chiral- antichiral metamaterials strained along the chiral direction at 0.0%, 6.7%, 14.6% and 20.5% level. Figure 7 (i–l) show the y-z view of the 3D chiral- chiral- antichiral metamaterials strained along the chiral

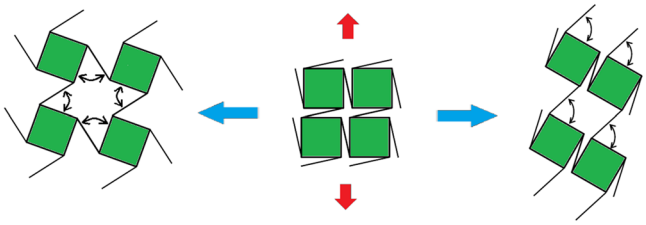

Figure 8. The competition deformation mechanisms: auxetic rotating mechanism without side deformation restriction, and shear deformation due to side deformation restriction.

direction at 0.0%, 3.3%, 7.2% and 9.1% level, and Fig. 7 (m–p) show the z-x view of the 3D chiral- chiral- antichiral metamaterials strained along the antichiral direction at 0.0%, 4.6%, 11.5% and 17.2% level.

As to the deformation mechanisms of these two types of 3D chiral metamaterials, rotation of the cubic chiral nodes and bending of ligaments are predominant. (1) As to the 3D chiral- antichiral- antichiral metamaterials, compression-shrinkage and tensile-expanding deformation mechanisms are dominant, where the rotation and bending of chiral-chiral and chiral-antichiral ligament-node pairs will results in auxetic deformation behaviors; (2) As to 3D chiral-chiral-antichiral metamaterials, which can be viewed as cubic solid medium cut out with four-pointed planar star pore systems from two perpendicular directions, where the horizontally inclined ligaments undergo a higher degree of flexural deformation than their vertically inclined counterparts, meaning the rotational symmetry of order four is not being preserved. As shown in Fig. 8, two main competing simplified deformation mechanisms are identified for the chiral-chiral structures of chiral-chiral-antichiral metamaterials, (a) the auxetic rotation deformation mechanism, where both ligaments and nodes rotate by the same amount, producing a negative Poisson ratio −1; (b) the shear-directed deformation mechanism results in a non-zero shear coefficient and a Poisson's ratio of zero[51,52]. In the compression-shearing experiments shown in Fig. 3 (d–f), graphite sheets with quite low friction coefficients (<=0.005) are attached onto the compression contacting surfaces for minimizing the friction force, and side shearing deformation mechanism is predominant resulting in zero Poisson's ratio. In the *in-situ* uniaxial tensile experimental tests shown in Fig. 7 (e–h), the auxetic rotating mechanism becomes more active due to the restriction of shear deformation imposed by the uniaxial loading boundary conditions, and thus the system has an overall negative Poisson's ratio. As tensile strain increases, the Poisson's ratio gradually becomes even more negative as the rotation of nodes becomes more predominant, resulting in deformation mechanism from shearing deformation dominant towards auxetic rotating deformation dominant.

With the progress of micro- and nano- manufacturing techniques, the proposed 3D chiral metamaterials show promising performances for future industrial applications, such as: nano chiral metatllic glass with extensive hardening and large ductility, sound absorption and vibration attenuation metamaterials, morphing structures, optical chiral metamaterials, shape memory actuators and biomechanical devices.

Conclusions

In this paper, two types of innovative 3D chiral metamaterials are proposed, namely chiral- chiral- antichiral and chiral- antichiral- antichiral metamaterials. Firstly, two series of 3D chiral metamaterials with different geometrical parameters are designed, and the 3D chiral metamaterials samples are fabricated with Selective Laser Sintering (SLS) nylon sintering techniques, and *in-situ* compression test are performed for studying the mechanical properties and deformation mechanisms of 3D chiral metamaterials. Secondly, *in-situ* uniaxial tensile tests are performed for exploring the competitions between two main types of deformation mechanisms: shearing deformation and auxetic rotating deformation of chiral structures.

The proposed 3D chiral metamaterials represents a series of metamaterials with robust microstructures design feasibilities. With the progress of micro- and nano- manufacturing techniques, the proposed 3D chiral metamaterials show promising performances for future industrial applications, such as: nano chiral metatllic glass with extensive hardening and large ductility, sound absorption and vibration attenuation metamaterials, morphing structures, optical chiral metamaterials, shape memory actuators and biomechanical devices.

References

1. Meza, L. R. *et al.* Resilient 3D hierarchical architected metamaterials. *Proc Nat Acad Sci USA* **112**(37), 11502–11507 (2015).
2. Gu, X. W. & Greer, J. R. Ultra-strong architected Cu meso-lattices. *Extreme Mech. Lett.* **2**, 7–14 (2015).
3. Meza, L. R., Das, S. & Greer, J. R. Strong, lightweight, and recoverable three-dimensional ceramic nanolattices. *Science* **345**(6202), 1322–1326 (2014).
4. Gu, X. W. *et al.* Mechanisms of Failure in Nanoscale Metallic Glass. *Nano Lett.* **14**(10), 5858–5864 (2014).
5. Zheng, X. Y. *et al.* Ultralight, ultrastiff mechanical metamaterials. *Science* **344**(6190), 1373–1377 (2014).
6. Zhu, R., Liu, X. N., Hu, G. K., Sun, C. T. & Huang, G. L. Negative refraction of elastic waves at the deep-subwavelength scale in a single-phase metamaterial. *Nature Comm.* **5**, 5510 (2014).
7. Wong, Z. J. *et al.* Optical and acoustic metamaterials: superlens, negative refractive index and invisibility cloak. *J. Optics* **19**, 084007 (2017).
8. Smith, D. R., Vier, D. C., Koschny, T. & Soukoulis, C. M. Electromagnetic parameter retrieval from inhomogeneous metamaterials. *Phys. Rev. E* **71**, 036617 (2015).
9. Shelby, R. A., Smith, D. R. & Schultz, S. Experimental Verification of a Negative Index of Refraction. *Science* **292**(5514), 77–79 (2001).

10. Wang, Q. M. *et al*. Lightweight Mechanical Metamaterials with Tunable Negative Thermal Expansion. *Phys. Rev. Lett.* **117**, 175901 (2016).
11. Wu, L. L., Li, B. & Zhou, J. Isotropic Negative Thermal Expansion Metamaterials. *ACS Appl. Mater. Interfaces* **8**(27), 17721 (2016).
12. Chen, L. *et al*. Evidence of near-infrared partial photonic bandgap in polymeric rod-connected diamond structures. *Adv. Funct. Mater.* **20**, 1038–1052 (2010).
13. Zhang, S. *et al*. Negative Refractive Index in Chiral Metamaterials. *Phys. Rev. Lett.* **102**, 023901 (2009).
14. Vignolini, S. *et al*. A 3D optical metamaterial made by self-assembly. *Adv. Mater.* **24**, OP23–OP27 (2012).
15. Soukoulis, C. M. & Wegener, M. Past achievements and future challenges in the development of three-dimensional photonic metamaterials. *Nat. Photonics* **5**(9), 523–530 (2011).
16. Love, A. *A treatise on the mathematical theory of elasticity*. (Dover Publications, New York, 1944).
17. Novak, N., Vesenjak, M. & Ren, Z. Auxetic Cellular Materials—A Review. *Strojniškivestnik - J. Mech. Eng.* **62**(9), 485–493 (2016).
18. Kelvin, L. Baltimore lectures on molecular dynamics and the wave theory of light. *C. J. Clay and Sons. London* (1904).
19. Wang, J. S. *et al*. Hierarchical chirality transfer in the growth of Towel Gourd tendrils. *Sci. Rep.* **3**, 3102 (2013).
20. Chandraseker, K., Mukherjee, S., Paci, J. T. & Schatz, G. C. An atomistic-continuum Cosserat rod model of carbon nanotubes. *J. Mech. Phys. Solids* **57**, 932–958 (2009).
21. Ye, H. M. *et al*. Surface Stress Effects on the Bending Direction and Twisting Chirality of Lamellar Crystals of Chiral Polymer. *Macromolecules* **43**(13), 5762–5770 (2010).
22. Schwaiger, S., Rottler, A. & Mendach, S. Rolled-Up Metamaterials. *Adv. OptoElectron*. 782864 (2012).
23. Valev, V. K., Baumberg, J. J., Sibilia, C. & Verbiest, T. Chirality and Chiroptical Effects in Plasmonic Nanostructures: Fundamentals, Recent Progress, and Outlook. *Adv. Mater.* **25**, 2517–2534 (2013).
24. Pendry, J. B. A Chiral Route to Negative Refraction. *Science* **306**, 1353–1355 (2004).
25. Tang, Y. & Cohen, A. E. Enhanced Enantioselectivity in Excitation of Chiral Molecules by Superchiral Light. *Science* **332**, 333–336 (2011).
26. Kaschke, J., Gansel, J. K. & Wegener, M. On metamaterial circular polarizers based on metal N-helices. *Opt. Express* **20**(23), 26012–26020 (2012).
27. Gansel, J. K. *et al*. Gold Helix Photonic Metamaterial as Broadband Circular Polarizer. *Science* **325**, 1513 (2009).
28. Li, W. *et al*. Circularly Polarized Light Detection with Hot Electrons in Chiral Plasmonic Metamaterials. *Nat. Commun.* **6**, 8379 (2015).
29. Prall, D. & Lakes, R. S. Properties of a chiral honeycomb with a poisson's ratio of – 1. *Int. J. Mech. Sci.* **39**(3), 305–314 (1997).
30. Alderson, A. *et al*. Elastic constants of 3-, 4- and 6-connected chiral and anti-chiral honeycombs subject to uniaxial in-plane loading. *Comp. Sci. Tech.* **70**, 1042–1048 (2010).
31. Chen, Y. J., Scarpa, F., Liu, Y. J. & Leng, J. S. Elasticity of anti-tetrachiral anisotropic lattices, Int. *J. Solids Struc.* **50**, 996–1004 (2013).
32. Li, H. M. *et al*. In plane mechanical properties of tetrachiral and antitetrachiral hybrid metastructures. *Appl. Mech.T-ASME* **84**(8), 081006 (2017).
33. Wu, W. W. *et al*. Mechanical properties of hierarchical anti-tetrachiral metastructures. *Extreme Mech. Lett.* **16**, 18–32 (2017).
34. Wu, W. *et al*. Mechanical properties of anti-tetrachiral auxetic stents, Comp. *Struct.* **185**, 381–392 (2018).
35. Cosserat, E. & Cosserat, F. *Theorie des Corps Deformables*. A (Hermann, Paris, 1909).
36. Lakes, R. S. Foam Structures with a Negative Poisson's Ratio. *Science* **235**, 1038–1040 (1987).
37. Eringen, A. C. Linear Theory of Micropolar Elasticity. *J. Math. Mech.* **15**, 909–923 (1966).
38. Liu, X. N., Huang, G. L. & Hu, G. K. Chiral effect in plane isotropic micropolar elasticity and its application to chiral lattices. *J. Mech. Phys. Solids* **60**, 1907–1921 (2012).
39. Chen, Y., Liu, X. N., Hu, G. K., Sun, Q. P. & Zheng, Q. S. Micropolar model of tetrachiral lattices. *Proc. R. Soc. A* **470**, 20130734 (2013).
40. Spadoni, A. & Ruzzene, M. Elasto-static micropolar behavior of a chiral auxetic lattice. *J. Mech. Phys. Solids* **60**, 156–171 (2012).
41. Kang, S. H. *et al*. Buckling-Induced Reversible Symmetry Breaking and Amplification of Chirality Using Supported Cellular Structures. *Adv. Mater.* **25**(24), 3380–3385 (2013).
42. Shan, S. *et al*. Harnessing Multiple Folding Mechanisms in Soft Periodic Structures for Tunable Control of Elastic Waves. *Adv. Funct. Mater.* **24**, 4935–4942 (2014).
43. Ha, C. S., Plesha, M. E. & Lakes, R. S. Chiral three-dimensional lattices with tunable Poisson's ratio. *Smart Mater. Struct.* **25**, 054005 (2016).
44. Chan, S. H., Plesha, M. E. & Lakes, R. S. Chiral three-dimensional isotropic lattices with negative Poisson's ratio. *Phys Status Solidi B* **253**(7), 1243–1251 (2016).
45. Fu, M. H., Zheng, B. B. & Li, W. H. A novel chiral three-dimensional material with negative Poisson's ratio and the equivalent elastic parameters. *Comp. Struct.* **176**, 442–448 (2017).
46. Smith, C. W., Grima, J. N. & Evans, K. E. A novel mechanism for generating auxetic behaviour in reticulated foams: missing rib foam model. *Acta Mater.* **48**(17), 4349–4356 (2000).
47. Jiang, Y. Y. & Li, Y. N. 3D Printed Chiral Cellular Solids with Amplified Auxetic Effects Due to Elevated Internal Rotation. *Adv. Eng. Mater.* **2017**, 1600609 (2017).
48. Jiang, Y. Y. & Li, Y. N. Novel 3D-Printed Hybrid Auxetic Mechanical Metamaterial with Chirality-Induced Sequential Cell Opening Mechanisms. *Adv. Eng. Mater.* **10**, 1700744 (2017).
49. Frenzel, T., Kadic, M. & Wegener, M. Three-dimensional mechanical metamaterials with a twist. *Science* **358**, 1072 (2017).
50. Sha, Z. D. *et al*. Metallic glass-based chiral nanolattice: Light weight, auxeticity, and superior mechanical properties. *Mater. Today* **20**(10), 569–576 (2017).
51. Grima, J. N. *University of Exeter*, Ph.D. Thesis, (United Kingdom, 2000).
52. Cicala, G. *et al*. Hexachiral truss-core with twisted hemp yarns: Out-of-plane shear properties. *Compos. Struct.* **94**, 3556–3562 (2012).

Acknowledgements

This research is supported by the National Natural Science Foundation of China (Grant No. 11702023), and National Natural Science Foundation of China (Grant No. 11632010).

Author Contributions

The concept of 3D chiral systems was developed by W. Wu. The experiments were performed by D. Qi, Y. Niu and H. Liao, the simulations were performed by G. Qian and L. Geng, W. Wu and J. Liang wrote the main manuscript text, while the figures were prepared by D. Qi, Y. Niu, H. Liao and G. Qian. L.Geng contributed to the discussion of the manuscript mainly on FEA simulation aspects of the work involved. The work was supervised by W. Wu, H. Liao and G. Qian. All authors reviewed the manuscript before submission.

Additional Information

Competing Interests: The authors declare no competing interests.

Publisher's note: Springer Nature remains neutral with regard to jurisdictional claims in published maps and institutional affiliations.